

Polymer Chemistry

Accepted Manuscript



This is an *Accepted Manuscript*, which has been through the Royal Society of Chemistry peer review process and has been accepted for publication.

Accepted Manuscripts are published online shortly after acceptance, before technical editing, formatting and proof reading. Using this free service, authors can make their results available to the community, in citable form, before we publish the edited article. We will replace this *Accepted Manuscript* with the edited and formatted *Advance Article* as soon as it is available.

You can find more information about *Accepted Manuscripts* in the [Information for Authors](#).

Please note that technical editing may introduce minor changes to the text and/or graphics, which may alter content. The journal's standard [Terms & Conditions](#) and the [Ethical guidelines](#) still apply. In no event shall the Royal Society of Chemistry be held responsible for any errors or omissions in this *Accepted Manuscript* or any consequences arising from the use of any information it contains.

ARTICLE

Backbone Rigidity and Its Influences on the Morphology and Charge Mobility of FBT Based Conjugated Polymers

Kuan-Yi Wu^a, Chun-Chieh Chiu^a, Wei-Tsung Chuang^b, Chien-Lung

Wang^{a*} and Chain-Shu Hsu^{a*}

Cite this: DOI: 10.1039/x0xx00000x

Received 00th January 2012,
Accepted 00th January 2012

DOI: 10.1039/x0xx00000x

www.rsc.org/

A series of three **PVTh₄FBT** polymers containing different alkyl side chain placements were synthesized. The thermochromic behaviors and the DFT calculations indicated that the backbone coplanarity and rigidity of the **PVTh₄FBT** polymers can be effectively modulated through adjusting the side chain position and density. Higher ordered and better oriented edge-on lamellar packing was formed by **P1**, which possesses the most rigid backbone among the three polymers and pre-aggregates in the solution. **P1** also delivered the highest hole mobility (0.26 cm²V⁻¹s⁻¹) among the three analogues because its thin-film morphology is in favor of charge transport.

Introduction

Solution-processed organic field-effect transistors (OFETs) have attracted substantial research attention for their potential applications as low-cost components in large-area flexible electronics¹⁻³. Significant progresses in molecular design, and device physics have led to polymer-based OFETs with charge mobility (μ) over 1.0 cm²/Vs.

Based on the Marcus theory, low reorganization energies (λ_{reorg}) and high degrees of intermolecular electronic coupling are conducive for conjugated molecules to reach high μ .⁴⁻⁹ Via fusing the neighboring aromatic units, chemical rigidification inhibits the inter-annular rotation. Thus, conjugated systems with multifused heteroarenes possess reduced λ_{reorg} s, and better coplanarity. Along with suitable lateral solubilizing side chains, effective intermolecular electronic coupling and high μ have been reported.^{10, 11} Recently, non-fused conjugated polymers also delivered comparable and even higher μ s than their fused counterparts.¹²⁻¹⁴ Without chemical rigidification, thiophene-based conjugated backbones are easily distorted through inter-annular rotation, as indicated by the low twist glass transition temperatures of poly(3-alkylthiophene)s.¹⁵ The low energy barriers for the inter-annular rotation and the low conformational preferences of many non-fused Donor-Acceptor (D-A) backbones also lead to multiple possible spatial arrangements of the conjugated backbones and affect the polymer packing in the condensed phases.¹⁶ Moreover, the backbone coplanarity and packing order of non-fused conjugated polymers are more sensitive

to the bulkiness, chain lengths and attachment densities of the alkyl side chains.¹⁷⁻²⁰ To physically rigidify the non-fused backbones, the stability of the coplanar state, in other words, the rigidity of the conjugated backbone should be modulated.

The rigidity of the conjugated backbone can be affected by the main chain structure, as well as the solubilizing side chains. 5,6-difluorobenzo-2,1,3-thiadiazole (FBT) based D-A copolymers, are conjugated polymers with high performances.^{14, 21-23} However, the ways of modulating the rigidity of the FBT polymers, and the influences of the backbone rigidity to the packing order and the charge mobility have not been carefully studied. Since theoretically, the FBT unit is considered as inefficient at locking the conformations,¹⁶ the backbone properties of the non-fused FBT polymers can be critical to the solid-state order and the OFET performances. Herein, a family of 5,6-difluorobenzo-2,1,3-thiadiazole-4,7-diyl (FBT) - bis(bithienylene)vinylene **PVTh₄FBT** copolymers - **P1**, **P2**, and **P3** (Scheme 1) were synthesized. All three polymers share the same backbone structure, but **P1** and **P2** are different in their side chain positions, and **P3** has a higher side chain density than the other two. The influences of the vinylene group, along with the position and attached density of the side chains, to the backbone rigidity, solid-state morphology and OFET mobility were investigated. The results show that the backbone rigidity of **PVTh₄FBT** can be effectively modulated through adjusting the side chain position and density. More importantly, the solid-state order and crystal orientations of the **PVTh₄FBT** polymers were affected by the backbone properties. The highest backbone rigidity of **P1**

resulted in the most ordered and well-oriented edge-on lamellae on the substrate, which rendered **P1** the highest μ_h of among the three polymers.

Experimental Session

General Measurement and Characterization: All chemicals were purchased from Aldrich or Acros and used as received unless otherwise specified. Synthesis and characterizations of the FBT monomers, DTV monomers and polymers were summarized in the supporting information. FBT-1 was synthesized according to the literature.¹⁴ ¹H and ¹³C NMR spectra were measured using a Varian 300 MHz instrument spectrometer. Molecular weights and polydispersity indices (PDI) of the polymers were determined by high temperature (120 °C) gel permeation chromatography (GPC) using a Viscotek module-350 system with polystyrene as standard and 1,2,4-trichlorobenzene (TCB) as eluent. Differential scanning calorimetry (DSC) was measured on a TA Q200 Instrument and thermogravimetric analysis (TGA) was recorded on a Perkin Elmer Pyris under nitrogen atmosphere at a heating rate of 10 °C min⁻¹. Absorption spectra were collected on a HP8453 UV-vis spectrophotometer. The electrochemical cyclic voltammetry (CV) was conducted on a CH Instruments Model 611D. A carbon glass coated with a thin polymer film was used as the working electrode and Ag/Ag⁺ electrode as the reference electrode, while 0.1 M tetrabutylammonium-hexafluorophosphate (Bu₄NPF₆) in acetonitrile was the electrolyte. CV curves were calibrated using ferrocene as the standard, whose oxidation potential is set at -4.8 eV with respect to zero vacuum level. The E_{HOMO} s were derived from the equation $E_{\text{HOMO}} = - (E_{\text{ox}}^{\text{onset}} - E_{(\text{ferrocene})}^{\text{onset}} + 4.8)$ eV. The E_{LUMO} s were derived from the equation $E_{\text{LUMO}} = - (E_{\text{red}}^{\text{onset}} - E_{(\text{ferrocene})}^{\text{onset}} + 4.8)$ eV. A Veeco Diinova atomic force microscope (AFM) in the tapping mode was used to characterize surface morphology of the polymer thin films. The Grazing Incidence X-ray diffraction (GIXD) patterns of **PVTh₄FBT** polymers were recorded at the BL01C2 beamline of the National Synchrotron Radiation Research Center (NSRRC) in Taiwan. The ring energy of NSRRC was operated at 1.5 GeV with a typical current of 300 mA. The wavelength of the incident X-rays was 1.0332 Å (12.0 keV), delivered from the superconducting wavelength-shifting magnet, and a Si(111) double-crystal monochromator. The samples were placed horizontally on a sample stage. With an incident angle 0.2°, GIXD was conducted and the pattern was collected with the detector system included a CMOS flat panel X-ray detector C9728DK. The scattering wave vector, defined as $q = 4\pi\sin\theta/\lambda$ (with 2θ the scattering angle), was calibrated using silver behenate, sodalite, and silicon powders, respectively. The thin films used in the AFM and GIXD measurements were prepared according to the processes used in the OFET fabrication.

Computational Details: Quantum-chemical calculations were performed with the Gaussian09 suite employing the B3LYP density functional in combination with the 6-311G(d,p) basis set. Geometry optimizations were performed with tight SCF and convergence criteria and an ultrafine integration grid by applying the GEDIIS optimization algorithm. The minimum nature of each stationary point was confirmed by a frequency analysis. The torsion potential energy surface was produced by the scan of single-point energy

calculations at the B3LYP/6-311G(d,p) level, and the dihedral angle θ_2 was stepped in 10° increments from the optimized geometry.

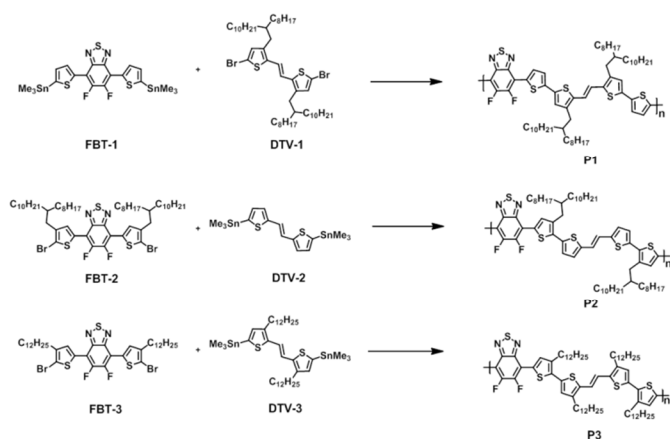
OFET Fabrication: An n-type heavily doped Si wafer with a SiO₂ layer of 300 nm and a capacitance per unit area of 11 nF cm⁻² was used as the gate electrode and dielectric layer. Thin films (40–60 nm in thickness) of polymers were deposited on the octadecyltrichlorosilane (ODTS)-treated SiO₂/Si substrates by spin-coating the ODCB solutions (2.5 mg mL⁻¹ and 5 mg mL⁻¹) or the TCB solutions (2.5 mg mL⁻¹) of the polymers. Then, the thin films were annealed at 200 °C in nitrogen atmosphere for 30 min. Gold source and drain electrodes (30 nm in thickness) were deposited by vacuum evaporation on the organic layer through a shadow mask, affording a bottom-gate, top-contact device configuration. Electrical measurements of OFET devices were carried out at room temperature in nitrogen using a 4156C, Agilent Technologies. The field-effect mobility was calculated in the saturation regime by using the equation $I_{\text{DS}} = (\mu WC_i/2L)(V_G - V_T)^2$, where I_{DS} is the drain-source current, μ is the field-effect mobility, W is the channel width (1 mm), L is the channel length (0.1 mm), C_i is the capacitance per unit area of the gate dielectric layer, and V_G is the gate voltage.

Result and Discussion

Synthesis and Thermal Analysis

The synthetic routes of the **PVTh₄FBT** polymers are depicted in the **Scheme 1**. Pd-catalyzed Stille-coupling copolymerization of 5,6-difluoro-4,7-bis(5-(trimethylstannyl)-thiophen-2-yl)benzo[c][1,2,5]thiadiazole (**FBT-1**) and (*E*)-1,2-bis(5-bromo-3-(2-octyl dodecyl)thiophen-2-yl)ethene (**DTV-1**) afforded the formation of **P1** in 73% yield; copolymerization of 4,7-bis(5-bromo-4-(2-octyl dodecyl)thiophen-2-yl)-5,6-difluoro-benzo[c][1,2,5]thiadiazole (**FBT-2**) and (*E*)-1,2-bis(5-(trimethylstannyl)thiophen-2-yl)ethene (**DTV-2**) resulted in the formation of **P2** in 63% yield; and copolymerization of 4,7-bis(5-bromo-4-dodecylthiophen-2-yl)-5,6-difluorobenzo[c][1,2,5]thiadiazole (**FBT-3**) and (*E*)-1,2-bis(3-dodecyl-5-(trimethylstannyl)thiophen-2-yl)ethene (**DTV-3**) afforded the formation of **P3** in 39% yield. The molecular weights and polydispersity (PDI) of the polymers are $M_n = 32.3$ kDa, (PDI = 2.8) for **P1**, $M_n = 38.2$ kDa (PDI = 2.1) for **P2**, $M_n = 11.2$ kDa (PDI = 1.5) for **P3**. The **PVTh₄FBT** polymers exhibited good thermal stability with 1% weight loss temperatures (T_{d5}) over 360 °C measured by thermogravimetric analysis (Figure S1). The polymers were heated up to 300 °C to avoid thermal degradation in the differential scanning calorimetry (DSC) analysis (Figure S2). The melting temperatures (T_m) and the crystallization temperature of **P2** were observed at 262 °C and 232 °C, respectively, but no phase transition was found for **P1** and **P3** below 300 °C. Since the grazing-incidence X-ray diffraction (GIXD) measurements discussed below confirmed that **P1-P3** all form ordered solid-state phases, the T_m s of the ordered phases of **P1** and **P3** should be above the upper temperature limit of the DSC measurements (300 °C), and thus, the melting processes of the two polymers were not detected. The lower T_m of **P2** indicated that the bulky 2-octyl dodecyl (OD) substituent at the 4' position (see Figure S3 for number code) of the (*E*)-1,2-bis(2,2'-bithiophen-5-

yl)ethene structural unit, decreasing the thermal stability of the crystalline state. Since the three polymers share the same backbone, the DSC results gave the first indication that the alkyl chain position affects the backbone rigidity and the phase stability of the **PVTh₄FBT** polymers.



Scheme 1. Synthetic procedures of **PVTh₄FBT** polymers. Reagents and conditions: (i) tris(dibenzylideneacetone)dipalladium(0), tri(o-tolyl)phosphine, chlorobenzene, 120 °C, 48 hrs.

Optical and Electrochemical Properties

The optical behaviors of the polymers were investigated by ultraviolet-visible (UV-Vis) spectroscopy in dilute *o*-dichlorobenzene (ODCB) solutions and as thin films on glass. The characteristics of UV-Vis spectrum of the **PVTh₄FBT** polymers are summarized in Table 1. As shown in Figure 1, the absorption bands with λ_{max} around 450 nm can be attributed to localized $\pi - \pi^*$ transition. The λ_{max} of the photo-induced intramolecular charge transfer (ICT) absorptions of **P1** is at 655 nm. Compared to λ_{max} of **PTh₄FBT** (the polymer analogue without the vinylene structural unit) in our previous study,²² the absorption of **P1** bathochromic shifts for 80 nm. Thus, the vinylene unit effectively increases the conjugation length of the polymer. Compared the ICT band of **P1**, the hypsochromic shifts of the **P2** and **P3** absorptions (Table 1) suggest the decreases in the effective conjugation lengths.²⁴ Since the three polymers share the same conjugated backbone, the disruption of the effective conjugation was attributed to the decreased backbone coplanarity caused by the OD side chains near the inter-thienyl bond (in the case of **P2**), and the increased side chain density (in the case of **P3**). Pre-aggregation of the copolymers in the ODCB solutions are evident at room temperature, since the 710 nm absorption shoulder observed in the thin films can also be found in the solutions. The weakest absorption shoulder of **P3** in solution indicates that the high side chain density may prevent the effectively inter-chain interactions in the solution. Deduced from cyclic voltammetry measurements (Figure S4), the E_{HOMOS} and E_{LUMOS} of the polymers were also summarized in Table 1.

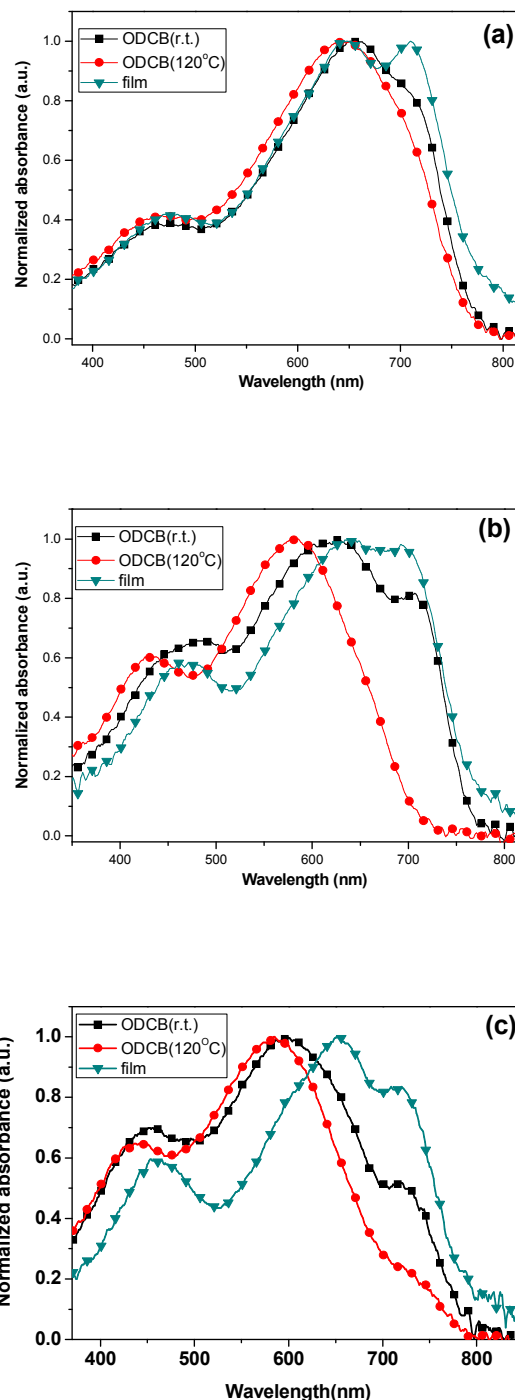


Figure 1. Normalized UV-vis absorption spectra of (a) **P1**, (b) **P2** and (c) **P3** in the ODCB solution at room temperature (black square), at 120 °C (red circle), and in the thin-film state (green triangle).

Table 1. Optical and electrochemical properties of PVTh₄FBT polymers

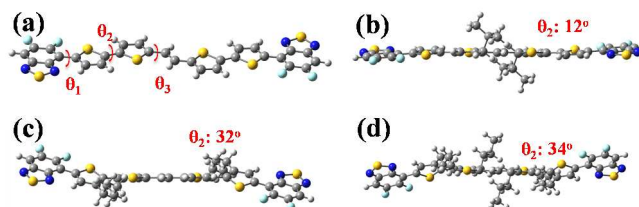
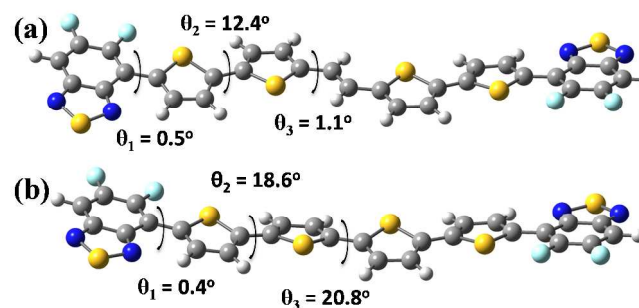
Polymer	λ_{\max} (nm)		$E_{g,opt}$ (eV)	E_{HOMO} (eV)	E_{LUMO} (eV)
	Solution	Film			
P1	652, 704	652, 710	1.54	-5.23	-3.43
P2	620, 704	640, 706	1.57	-5.31	-3.02
P3	600, 706	655, 706	1.54	-5.27	-3.23

The backbone rigidities of the polymers were further evaluated through thermochromic experiments. At a solution temperature of 120 °C, the three polymers responded differently to the thermal disturbance. The increased solution temperature resulted in only a 2 nm hypsochromic shift to the ICT band of **P1**, but 37 nm and 15 nm hypsochromic shifts to those of **P2** and **P3**. Therefore, the effective conjugation and backbone coplanarity of **P1** are much more difficult to be thermally disturbed than the other two. The increased solution temperature also disaggregated the PVTh₄FBT polymers in the solution, as indicated by the decreased intensity of the 710 nm absorption bands. The photophysical behaviors of the PVTh₄FBT polymers thus reveals the strong influences of the side chain position and side chain density to the backbone properties of the polymers.

Theoretical Calculation

Using Gaussian 09, density functional theory (DFT) calculations were performed on the simplified repeat units of the polymers at the B3LYP/6-311G (d,p) level.^{25, 26} The molecular segment of the PVTh₄FBT polymer shown in Figure 2a was selected for the calculations to emphasize the influences of the alkyl side chains to the interannular dihedral angles ($\theta_1 - \theta_3$) and the coplanarity of the backbone. To first evaluate the influence of the vinylene group, comparison of the PVTh₄FBT and PTh₄FBT backbones were made under the condition where the alkyl side chains were excluded. As shown in Figure 3, the smaller θ_2 and θ_3 angles of PVTh₄FBT indicate its better backbone coplanarity than that of PTh₄FBT. The improved coplanarity was attributed that the vinylene unit reduces the interannular steric hindrance.^{27-31,32}

The optimized conformations of the molecular segments of **P1**, **P2** and **P3** are shown in Figure 2b-2d. The dihedral angles ($\theta_1 - \theta_3$) in the optimized geometries of the three polymers were summarized in Table 2. The alkyl side chains degraded the backbones coplanarity as indicated by the increased interannular dihedral angles. The degree of interannular torsion depends on the alkyl side chain placements. As can be seen in the cases of **P1** and **P3**, the alkyl groups closer to the vinylene unit (4-position, see the number codes for the substituents in Figure S3) is less effective in distorting the backbone, while those closer to the inter-thienyl single bond (3'-postion) evidently increased θ_2 from 12° to over 32°.

**Figure 2.** (a) Illustration of the molecular segment of the PVTh₄FBT backbone and the interannular dihedral angles - θ_1 , θ_2 , and θ_3 . Side views of the optimized geometries of (b) **P1**, (c) **P2** and (d) **P3** at the B3LYP/6-311G(d,p) level of theory.**Figure 3.** The optimized geometries of (a) the PVTh₄FBT backbone and (b) the PTh₄FBT backbone at the B3LYP/6-311G(d,p) level of theory.**Table 2.** Calculated dihedral angles in the optimized geometries of **P1-P3**

Polymer	θ_1 (deg)	θ_2 (deg)	θ_3 (deg)
P1	0.5	12.0	2.2
P2	0.5	31.5	1.2
P3	0.4	34.1	3.0

The backbone rigidity was further investigated through the potential energy profiles of the molecular segments plotted in Figure 4. In this figure, $\theta_2 = 0^\circ$ corresponds to a fully planar conformation. The potential energy minima calculated for **P1**, **P2** and **P3** locate at $\theta_2 = 12^\circ$, 32° , and 34° , respectively, suggesting a gradual decrease in the backbone coplanarity. Upon rotation around the inter-thienyl bond, the potential energy increases, and attains a maximum E^* of $3.8 \text{ kcal mol}^{-1}$ for **P1** and $1.62\text{-}1.75 \text{ kcal mol}^{-1}$ for **P2** and **P3** at $\theta_2 = 90^\circ$. The increase of the potential energy upon the bond rotation indicates that the torsion of the backbone is energetically unfavorable. The highest E^* of **P1** thus represents its highest backbone rigidity. The calculations agree with the results in the UV-Vis absorption experiments, where **P1** demonstrates the highest effective conjugation length yet lowest sensitivity to the thermal agitation in the solution.

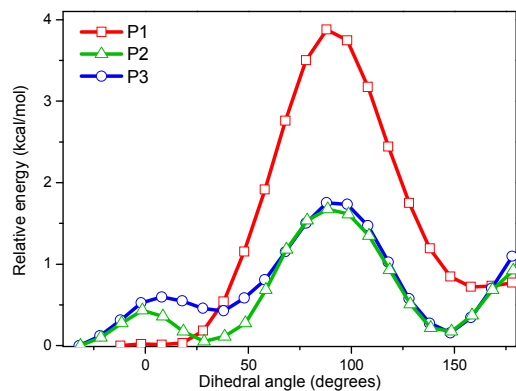


Figure 4. Potential energy profiles of the PVTh₄FBT segments at the B3LYP/6-311G(d,p) level of theory.

Grazing-Incidence X-ray Diffraction Analysis

To analyze the solid-state order and chain orientation in the thin-film, grazing-incidence X-ray diffraction (GIXD) measurements were performed on the thin films of the three polymers. The d -spacing and correlation length (L_{hkl}) deduced from the GIXD data are summarized in Table 3. In the GIXD patterns of the polymers shown in Figure 5, the scattering from lamellar stacking ($(h00)$ peaks) were observed along the q_z axis, and the scattering from π - π stacking were observed along the q_{xy} axis. Thus, the edge-on lamellar orientation is preferable for the three polymers. However, the polymers did show different degrees of packing order and the orientational uniformity. High order peaks up to (400) were observed for the lamellar packing of **P1** and **P2**, while only up to (300) were found for the **P3** thin film. Moreover, as shown in Figure 6, the broadness of the (100) peaks in the azimuthal scan increases from **P1** to **P2**, and to **P3**. Thus, the edge-on lamellar crystals of **P1** is more orderly oriented in the thin film than the other two. The lowest structural order of **P3** suggests that the increased side-chain density may deter the side-chain interdigitation and the registry between layers.¹⁸ Consequently, the lamellar packing of **P3** is not only less ordered, but also less oriented on the substrate. In contrast, as indicated by the thermochromic and the calculation results, **P1** possesses a more planar and rigid backbone than the other two. The highly ordered and well-oriented edge-on lamellae of **P1** is thus related to its coplanar conformation in solution. The relationship is in line with Chen's study about the Isoindigo-based polymers.³³

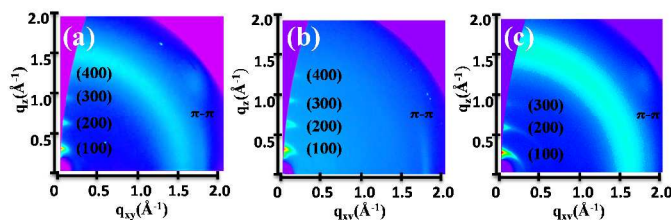


Figure 5. GIXD patterns of (a) **P1**, (b) **P2**, and (c) **P3**.

Table 3. Summary of the polymer packing parameters in the thin films determined from the GIXD patterns.

polymer	lamellar spacing (Å)	L_{100} (nm)	π - π spacing (Å)
P1	19.2	39	3.62
P2	19.7	28	3.62
P3	21.5	24	3.62

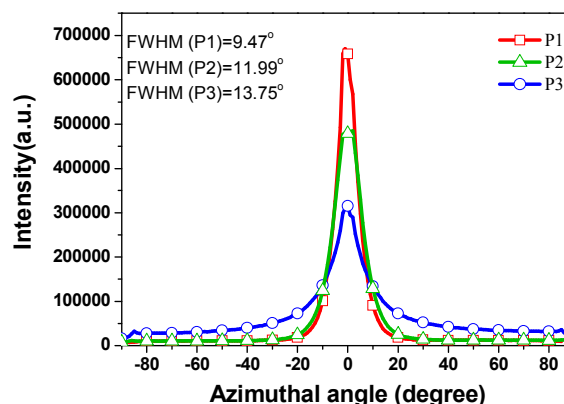


Figure 6. The azimuthal-angle scans for the (100) peaks in the GIXD patterns of the PVTh₄FBT polymers. The inset shows the full width at half maximum (FWHM) of each azimuthal scan.

OFET Performances

The charge transport properties of the PVTh₄FBT polymers were studied in OFET devices with a bottom-gate, top-contact configuration. The PVTh₄FBT polymers exhibited the p -channel OFET characteristics, as shown in Figure 7. The electric characters of the devices including μ_{h} , threshold voltage (V_{th}) and $I_{\text{on}}/I_{\text{off}}$ ratio extracted from the figures were summarized in Table 4. **P1** delivered the highest μ_{h} ($0.26 \text{ cm}^2\text{V}^{-1}\text{s}^{-1}$) among the three polymers, which can be attributed to its most ordered and oriented solid-state structure. Unexpectedly, despite **P2** has better solid-state order than **P3**, it delivered the lowest averaged μ_{h} of $0.027 \text{ cm}^2\text{V}^{-1}\text{s}^{-1}$. AFM revealed the surface topographies of the three polymer thin films (Figure S5). In Figure S5b, more grain boundaries were observed in **P2**. Because the presence of grain boundaries in the active layer is detrimental to charge mobility,³⁴⁻³⁷ improving the thin-film morphology of **P2** was attempted. As shown in Figure S6, through reducing the concentration of **P2** solutions from 5.0 to 2.5 mg mL^{-1} , film roughness (R_{RMS}) and the density of grain boundary of the **P2** thin film can be significantly decreased. Consequently, the characteristics of the **P2** OFET devices (Figure 7S) was improved and the μ_{h} was increased to 0.089-0.12 $\text{cm}^2\text{V}^{-1}\text{s}^{-1}$ (Table 5) due to the improved morphology.

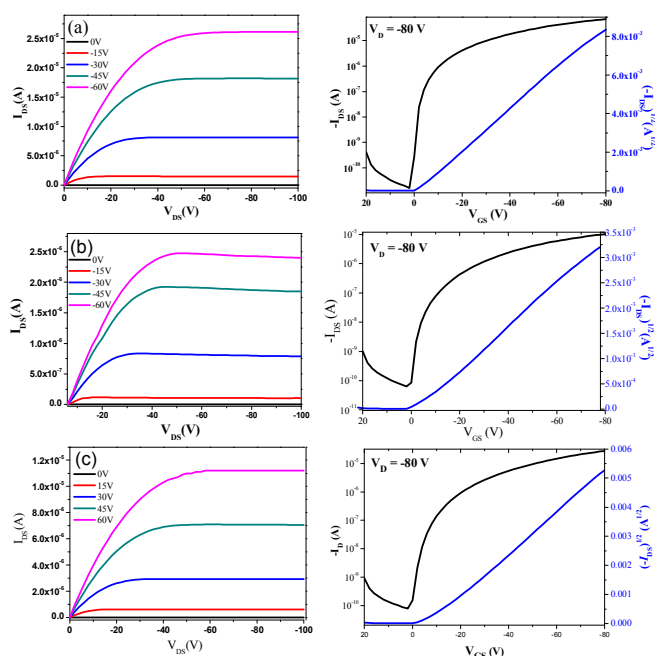


Figure 7. Transfer (right) and output (left) characteristics of the OFET devices of (a) **P1**, (b) **P2** and (c) **P3**

Table 4. OFET characteristics of the **PVTh₄FBT** polymers prepared from ODCB solution at a concentration of 5 mg mL⁻¹.

Polymer	$\mu_{h,avg}^a$ ($\mu_{h,highest}$) (cm ² V ⁻¹ s ⁻¹)	V_{th}^a (V)	I_{on}/I_{off}
P1	0.22 (0.26)	-2.6	10 ⁷
P2	0.027 (0.037)	-9.6	10 ⁵
P3	0.086 (0.12)	-9.8	10 ⁵ -10 ⁶

a) Averaged value of over five devices.

Table 5. OFET characteristics of **P2** prepared from reduced solution concentration (2.5 mg mL⁻¹)

Solvent	$\mu_{h,avg}^a$ ($\mu_{h,highest}$) (cm ² V ⁻¹ s ⁻¹)	V_{th}^a (V)	I_{on}/I_{off}
ODCB	0.089 (0.13)	-14.7	10 ⁴ -10 ⁵
TCB	0.12 (0.17)	-16.7	10 ³ -10 ⁵

a) Averaged value of over five devices.

Conclusions

In this study, vinylene group was introduced into a FBT based D-A polymer to physically planarize the conjugated backbone. The influences of alkyl chain position and density to the coplanarity and rigidity of the non-fused FBT based polymers were systematically compared in three **PVTh₄FBT** polymers. The thermochromic behaviors and DFT calculations indicated that the alkyl side chains close to the inter-thienyl bond and the high attached density increase

the inter-thienyl dihedral angle, and decrease the energy barrier of the interannual bond rotation. Consequently, the backbones of **P2** and **P3** are less coplanar and less rigid than **P1**. The backbone coplanarity in solution further affects the packing order and crystal orientation of the polymers in the thin film. GIXD results showed the **P1** formed the most ordered and oriented edge-on lamellar packing among the three polymers. Highest μ_h of 0.26 cm²V⁻¹s⁻¹ was delivered by **P1**, because its better solid-state order and suitable crystal orientation is conducive to the charge transfer in the OFET devices. Thus, the study revealed the critical role of the vinylene unit and the alkyl side chains on modulating the rigidity, packing order and OFET performances of the **FBT** based polymers.

Acknowledgements

This work is supported by the National Science Council and “ATP” of the National Chiao Tung University and Ministry of Education, Taiwan. The authors thank Prof. Keng S. Liang at Institute of Physics, Academia Sinica, Taiwan; Dr. Hwo-Shuenn Sheu at beamline BL01C; Dr. U-Ser Jeng at beamline BL23A of the National Synchrotron Radiation Research Center (NSRRC) in Taiwan for assistance with the XRD measurements.

Notes and references

^aDepartment of Applied Chemistry, National Chiao Tung University 1001 Ta Hsueh Road Hsin-Chu, 30010 (Taiwan)

*E-mail: kclwang@nctu.edu.tw and cshsu@mail.nctu.edu.tw

^bNational Synchrotron Radiation Research Center, 101 Hsin-Ann Road, Hsinchu Science Park, Hsinchu, 300, Taiwan.

Electronic Supplementary Information (ESI) available: The synthesis details, TGA measurement, DSC thermograms, cyclic voltammograms, AFM image, transistor data and calculated input profile of PTh₄VF₄FBT polymers can be found in the Supporting Information. See DOI: 10.1039/b000000x/

- A. C. Arias, J. D. MacKenize, I. McCulloch, J. Rivnay and A. Salleo, *Chem. Rev.*, 2010, 110, 3-24.
- J. Li, Y. Zhao, H. S. Tan, Y. Guo, C. A. Di, G. Yu, Y. Liu, M. Lin, S. H. Lim, Y. Zhou, H. Su and B. S. Ong, *Sci. Rep.*, 2012, 2, 754.
- H. Yan, Z. Chen, Y. Zheng, C. Newman, J. R. Quinn, F. Dotz, M. Kastler and A. Facchetti, *Nature*, 2009, 457, 679-686.
- Z. Chen, M. J. Lee, R. Shahid Ashraf, Y. Gu, S. Albert-Seifried, M. Meedom Nielsen, B. Schroeder, T. D. Anthopoulos, M. Heeney, I. McCulloch and H. Siringhaus, *Adv. Mater.*, 2012, 24, 647-652.
- J. Fan, J. D. Yuen, W. Cui, J. Seifter, A. R. Mohebbi, M. Wang, H. Zhou, A. Heeger and F. Wudl, *Adv. Mater.*, 2012, 24, 6164-6168.
- I. Kang, T. K. An, J. A. Hong, H. J. Yun, R. Kim, D. S. Chung, C. E. Park, Y. H. Kim and S. K. Kwon, *Adv. Mater.*, 2013, 25, 524-528.
- T. Lei, J. H. Dou and J. Pei, *Adv. Mater.*, 2012, 24, 6457-6461.
- Y. Liu, H. Wang, H. Dong, J. Tan, W. Hu and X. Zhan, *Macromolecules*, 2012, 45, 1296-1302.
- Y. Liu, Q. Shi, L. Ma, H. Dong, J. Tan, W. Hu and X. Zhan, *J. Mater. Chem. C*, 2014, 2, 9505-9511.
- J. Mei, Y. Diao, A. L. Appleton, L. Fang and Z. Bao, *J. Am. Chem. Soc.*, 2013, 135, 6724-6746.
- I. Osaka, T. Abe, S. Shinamura and K. Takimiya, *J. Am. Chem. Soc.*, 2011, 133, 6852-6860.
- J. H. Kim, D. H. Lee, S. Yang da, D. U. Heo, K. H. Kim, J. Shin, H. J. Kim, K. Y. Baek, K. Lee, H. Baik, M. J. Cho and D. H. Choi, *Adv. Mater.*, 2013, 25, 4102-4106.
- H. Chen, Y. Guo, G. Yu, Y. Zhao, J. Zhang, D. Gao, H. Liu and Y. Liu, *Adv. Mater.*, 2012, 24, 4618-4622.

14. Z. Chen, P. Cai, J. Chen, X. Liu, L. Zhang, L. Lan, J. Peng, Y. Ma and Y. Cao, *Adv. Mater.*, 2014, 26, 2586-2591.
15. K. Yazawa, Y. Inoue, T. Yamamoto and N. Asakawa, *Phys. Rev. B*, 2006, 74.
16. H. N. Tsao, D. M. Cho, I. Park, M. R. Hansen, A. Mavrinskiy, Y. Yoon do, R. Graf, W. Pisula, H. W. Spiess and K. Mullen, *J. Am. Chem. Soc.*, 2011, 133, 2605-2612.
17. Z. Bao and A. J. Lovinger, *Chem. Mater.*, 1999, 11, 2607-2612.
18. R. J. Kline, D. M. DeLongchamp, D. A. Fischer, E. K. Lin, L. J. Richter, M. L. Chabiny, M. F. Toney, M. Heeney and I. McCulloch, *Macromolecules*, 2007, 40, 7960-7965.
19. T. Prosa, M. Winokur and R. McCullough, *Macromolecules*, 1996, 29, 3654-3656.
20. X. Zhang, L. J. Richter, D. M. DeLongchamp, R. J. Kline, M. R. Hammond, I. McCulloch, M. Heeney, R. S. Ashraf, J. N. Smith and T. D. Anthopoulos, *J. Am. Chem. Soc.*, 2011, 133, 15073-15084.
21. H. Zhou, L. Yang, A. C. Stuart, S. C. Price, S. Liu and W. You, *Angew. Chem.*, 2011, 123, 3051-3054.
22. J. F. Jheng, Y. Y. Lai, J. S. Wu, Y. H. Chao, C. L. Wang and C. S. Hsu, *Adv. Mater.*, 2013, 25, 2445-2451.
23. L. Yang, J. R. Tumbleston, H. Zhou, H. Ade and W. You, *Energy Environ. Sci.*, 2013, 6, 316-326.
24. C. Yang, F. P. Orfino and S. Holdcroft, *Macromolecules*, 1996, 29, 6510-6517.
25. F. C. Grozema, P. T. Van Duijnen, Y. A. Berlin, M. A. Ratner and L. D. Siebbeles, *J. Phys. Chem. B*, 2002, 106, 7791-7795.
26. S. B. Darling and M. Sternberg, *J. Phys. Chem. B*, 2009, 113, 6215-6218.
27. T. Lei, X. Xia, J. Y. Wang, C. J. Liu and J. Pei, *J. Am. Chem. Soc.*, 2014, 136, 2135-2141.
28. N. B. Kolhe, A. Z. Ashar, K. S. Narayan and S. K. Asha, *Macromolecules*, 2014, 47, 2296-2305.
29. J. C. Speros, H. Martinez, B. D. Paulsen, S. P. White, A. D. Bonifas, P. C. Goff, C. D. Frisbie and M. A. Hillmyer, *Macromolecules*, 2013, 46, 5184-5194.
30. J. Shin, H. A. Um, D. H. Lee, T. W. Lee, M. J. Cho and D. H. Choi, *Polym. Chem.*, 2013, 4, 5688.
31. T. Lei, J. H. Dou, X. Y. Cao, J. Y. Wang and J. Pei, *J. Am. Chem. Soc.*, 2013, 135, 12168-12171.
32. J. Kim, B. Lim, K.-J. Baeg, Y.-Y. Noh, D. Khim, H.-G. Jeong, J.-M. Yun and D.-Y. Kim, *Chem. Mater.*, 2011, 23, 4663-4665.
33. M. S. Chen, J. R. Niskala, D. A. Unruh, C. K. Chu, O. P. Lee and J. M. J. Fréchet, *Chem. Mater.*, 2013, 25, 4088-4096.
34. H. Bronstein, J. M. Frost, A. Hadipour, Y. Kim, C. B. Nielsen, R. S. Ashraf, B. P. Rand, S. Watkins and I. McCulloch, *Chem. Mater.*, 2013, 25, 277-285.
35. A. Salleo, R. J. Kline, D. M. DeLongchamp and M. L. Chabiny, *Adv. Mater.*, 2010, 22, 3812-3838.
36. B. Friedel, C. R. McNeill and N. C. Greenham, *Chem. Mater.*, 2010, 22, 3389-3398.
37. R. Joseph Kline, M. D. McGehee and M. F. Toney, *Nature Mater.*, 2006, 5, 222-228.